BIOCHEMISTRY
including biophysical chemistry & molecular biology

ARTICLE

pubs.acs.org/biochemistry

Structural Basis for the Catalytic Mechanism of Aspartate Ammonia Lyase

Guntur Fibriansah,[†] Vinod Puthan Veetil,[‡] Gerrit J. Poelarends,*[,‡] and Andy-Mark W. H. Thunnissen*[,†]

[†]Department of Biophysical Chemistry, Groningen Biomolecular Sciences and Biotechnology Institute, University of Groningen, Nijenborgh 7, 9747 AG Groningen, The Netherlands

[‡]Department of Pharmaceutical Biology, Groningen Research Institute of Pharmacy, University of Groningen, Antonius Deusinglaan 1, 9713 AV Groningen, The Netherlands

Supporting Information

ABSTRACT: Aspartate ammonia lyases (or aspartases) catalyze the reversible deamination of L-aspartate into fumarate and ammonia. The lack of crystal structures of complexes with substrate, product, or substrate analogues so far precluded determination of their precise mechanism of catalysis. Here, we report crystal structures of AspB, the aspartase from *Bacillus* sp. YM55-1, in an unliganded state and in complex with L-aspartate at 2.4 and 2.6 Å resolution, respectively. AspB forces the bound substrate to adopt a high-energy, enediolate-like conformation that is stabilized, in part, by an extensive network of hydrogen bonds between residues Thr101, Ser140, Thr141, and Ser319 and the substrate's β-carboxylate group. Furthermore, substrate binding induces a large conformational change in the SS loop (residues G_{317}SSIMPGKVN_{326}) from an open conformation to one that closes over the active site. In the closed conformation, the strictly conserved SS loop residue Ser318 is at a suitable position to act as a catalytic base, abstracting the Cβ proton of the substrate in the first step of the reaction mechanism. The catalytic importance of Ser318 was confirmed by site-directed mutagenesis. Site-directed mutagenesis of SS loop residues, combined with structural and kinetic analysis of a stable proteolytic AspB fragment, further suggests an important role for the small C-terminal domain of AspB in controlling the conformation of the SS loop and, hence, in regulating catalytic activity. Our results provide evidence supporting the notion that members of the aspartase/fumarase superfamily use a common catalytic mechanism involving general base-catalyzed formation of a stabilized enediolate intermediate.

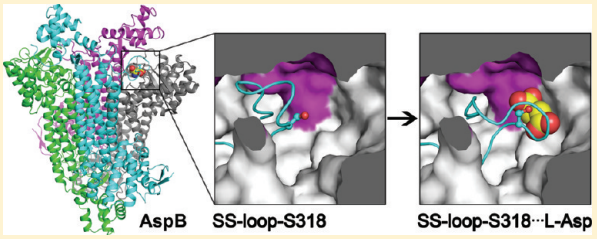

Aspartate ammonia lyases (also known as aspartases, EC 4.3.1.1) play an important role in microbial nitrogen metabolism by catalyzing the reversible conversion of L-aspartate to fumarate and ammonia. In industry, these enzymes are used as biocatalysts for the production of enantiopure L-aspartate, an important starting compound for the synthesis of food additives and artificial sweeteners.[1] Aspartases belong to the aspartase/fumarase superfamily, which also includes fumarase C, adenylosuccinate lyase, argininosuccinate lyase, δ1-crystallin, and 3-carboxy-*cis*,*cis*-muconate lactonizing enzyme, all of which have been structurally characterized by X-ray crystallography.[2−7] Members of this superfamily share a common tertiary and quaternary fold, as well as a similar active site architecture, despite the fact that pairwise sequence identities can be as low as 15%. They are biologically active as homotetramers and contain four composite active sites, each generated by conserved sequence motifs from three monomers. One of these conserved regions is a flexible loop of ~10 residues, containing the signature sequence GSSxxPxKxN (therefore named the SS loop), which for some aspartase/fumarase superfamily members has been shown to play an important role in substrate binding and catalysis.[3,8] Because of the structural similarities and because they all process succinyl-containing substrates leading to the formation of fumarate as the common product, it is believed that members of the aspartase/fumarase superfamily use a similar mechanism of catalysis involving general base-catalyzed formation of a stabilized enediolate (i.e., an aci-carboxylate) as a reaction intermediate.[3,6,8−11]

Aspartases have been purified and characterized from various Gram-negative and Gram-positive bacteria, including *Escherichia coli*, *Hafnia alvei*, *Pseudomonas fluorescens*, *Bacillus subtilis*, and *Bacillus* sp. YM55-1.[12−18] The aspartase from *E. coli*, AspA, has been studied most extensively, and its crystal structure has been elucidated.[19] AspA is allosterically activated by its substrate and Mg^{2+} ions, which are required for activity at alkaline pH. On the basis of biochemical and biophysical studies, and by relation of the enzyme to other members of the aspartase/fumarase superfamily, a reaction mechanism has emerged for the AspA-catalyzed deamination of L-aspartate. In this proposed mechanism, AspA catalyzes an anti-elimination reaction, where in the first step an active site base abstracts a proton from the Cβ atom of L-aspartate to form an enzyme-stabilized enediolate intermediate, which has two negative charges on its β-carboxyl group (i.e., an aci-carboxylate).[14,18,20] Collapse of this putative enediolate intermediate eliminates ammonia and yields the product,

Received: April 4, 2011
Revised: June 10, 2011
Published: June 10, 2011

fumarate. In the absence of structural data of AspA in complex with a substrate, product, or competitive inhibitor, the exact role of each active site residue in substrate binding and catalysis is not known yet. In particular, the identity of the catalytic base that abstracts the Cβ proton and the functional role of the SS loop have remained elusive.

The only other aspartase for which a crystal structure has been reported, albeit also in an unliganded state, is AspB from the thermophilic bacterium *Bacillus* sp. YM55-1.[21] A lack of allosteric regulation, combined with a high activity, excellent enantioselectivity, and relatively high thermostability, makes AspB very suitable as a biocatalyst in organic synthesis.[13] Notably, the broad nucleophile specificity of AspB in the reverse conjugate addition reaction, accepting alternative nucleophiles, such as methylamine, hydroxylamine, hydrazine, and methoxylamine, has been exploited for the synthesis of enantiopure N-substituted aspartic acids.[22] AspB is composed of 468 amino acid residues and is active as a homotetramer.[13] Site-directed mutagenesis, kinetic analysis, and structural modeling of substrate binding have provided insights into the functional role of various active site residues.[21,23] However, no obvious residue in the active site of AspB could be identified that may serve as a catalytic base in the first step of the proposed reaction mechanism. Also, the SS loop in the unliganded AspB structure (residues 317−328) is highly disordered, and like for AspA, its role in substrate binding and catalysis is unclear.

To improve our understanding of the functional roles of the active site residues and the SS loop in substrate binding and catalysis and to identify the general base catalyst in AspB, we have determined the crystal structure of wild-type AspB in complex with L-aspartate at 2.6 Å resolution. Comparison between this structure and a newly determined structure of unliganded AspB at 2.4 Å resolution reveals a large conformational change in the SS loop, from an open conformation in the absence of substrate to one in which it closes over the active site in the presence of substrate. The functional role of the SS loop in AspB, as well as that of the nearby C-terminal domain, was further analyzed by site-directed mutagenesis and limited proteolysis. The obtained results provide clear and new insights into the mechanism of catalysis by AspB and strongly suggest that Ser318 functions as the general base catalyst.

EXPERIMENTAL PROCEDURES

Expression Vector for Wild-Type AspB Production. To allow the overproduction of native, wild-type AspB (without any tags), the *aspB* gene was amplified by polymerase chain reaction (PCR) from plasmid pUCBA[24] using two synthetic primers and cloned in the pBAD/Myc-His A vector (Invitrogen). The forward primer (5′-ATA**CCATGG**ATACCGATGTTCG-3′) contains an *Nco*I restriction site (in bold) followed by 13 bases that correspond to the coding sequence of the *aspB* gene. The reverse primer (5′-CAT**CTGCAG**TTATTTTCTTCCAGCAATTCC-3′) contains a *Pst*I restriction site (in bold) followed by 18 bases that correspond to the complementary sequence of the *aspB* gene (including the stop codon sequence). The resulting PCR product and the pBAD/Myc-His A vector were digested with *Nco*I and *Pst*I restriction enzymes, purified, and ligated using T4 DNA ligase. Aliquots of the ligation mixture were transformed into competent *E. coli* TOP10 cells. Plasmid DNA was isolated from several transformants and analyzed by restriction analysis for the presence of the insert. The cloned *aspB* gene was sequenced to verify that no mutations had been introduced during the amplification of the gene. The newly constructed expression vector was named pBAD(AspB).

Expression and Purification of Wild-Type AspB. To produce native, wild-type AspB, the pBAD(AspB) plasmid was transformed into *E. coli* TOP10 cells. A single freshly transformed colony was picked using a sterile loop and used to inoculate 10 mL of LB/ampicillin medium. After overnight growth at 37 °C, the culture was diluted to an A_{600} of ∼0.02 in 1 L of LB/ampicillin medium in a 5 L Erlenmeyer flask. The culture was incubated at 37 °C with vigorous shaking until an A_{600} of 0.5−0.6 was reached, after which arabinose (0.04%, w/v) was added. Cells were incubated for an additional 8−10 h at 37 °C and then harvested by centrifugation (6000*g* for 15 min). The cell pellet was stored at −20 °C until further use.

In a typical purification experiment, ∼3 g of cell pellet (from a 1 L culture) was thawed and suspended in lysis buffer [50 mM Tris-HCl (pH 7.5), 100 mM NaCl, and 1 mM EDTA]. A protease inhibitor cocktail tablet (Roche Applied Sciences) was added to the mixture, and cells were treated (20 min on ice) with lysozyme (0.1 mg/mL). Cells were disrupted by sonication for 4 × 1 min (with a 4−6 min rest in between each cycle) at a 60 W output, after which unbroken cells and debris were removed by centrifugation (10000*g* for 50 min). The supernatant was collected, and L-aspartic acid was added to a final concentration of 0.1 M. Ammonium sulfate was added (11%, w/v), and the sample (∼20 mL) was heated at 72 °C for 9 min and then immediately cooled in an ice/water bath. Precipitated and denatured proteins were removed by centrifugation (10000*g* for 50 min), and the supernatant was loaded onto a phenyl-Sepharose column (Sigma-Aldrich) equilibrated with buffer A [50 mM Tris-HCl (pH 7.5), 1 mM EDTA, and 0.83 M $(NH_4)_2SO_4$]. The column was washed with 2 column volumes of buffer A, after which retained protein was eluted with buffer B [50 mM Tris-HCl (pH 7.5) and 1 mM EDTA]. Collected fractions were analyzed by sodium dodecyl sulfate−polyacrylamide gel electrophoresis (SDS−PAGE) and checked for activity. Fractions containing AspB were pooled, and the buffer was exchanged with buffer B. The protein sample was then loaded on a Q-Sepharose anion-exchange column (GE Healthcare), which had previously been equilibrated with buffer B. Retained protein was eluted with a linear concentration gradient of NaCl in buffer B (from 0 to 0.5 M). Fractions containing aspartase activity were pooled and concentrated to ∼4 mg/mL and then applied to a Sephadex S200 16/60 gel filtration column (GE Healthcare), which had previously been equilibrated with buffer C [25 mM Tris-HCl (pH 7.5)]. Fractions were analyzed by SDS−PAGE, and those that contained purified AspB were pooled and concentrated to ∼10 mg/mL. Freshly purified AspB was directly used for crystallization trials.

Cloning, Expression, and Purification of AspB-His Mutants. Site-directed mutagenesis was performed by overlap extension PCR[25] using plasmid pBAD(AspB-His) as the template.[22] The final PCR products were purified and cloned in the pBAD-myc-His A vector, which allows for the production of mutant proteins with a C-terminal polyhistidine tag. Each mutant gene was completely sequenced (with overlapping reads) to verify that only the intended mutation had been introduced. His-tagged mutant proteins were produced and purified using previously reported procedures.[22,23]

Enzyme Kinetic Measurements. Kinetic assays were performed at 25 °C in 50 mM NaH_2PO_4 buffer (pH 8.5) by

Table 1. Data Collection and Refinement Statistics

	AspB	AspB−L-Asp	chymo-AspB
Data Collection			
beamline (ESRF)	ID14-1	ID14-1	ID14-2
wavelength (Å)	0.9334	0.9334	0.9330
space group	*P*1	*P*1	$P2_1$
unit cell	*a* = 75.6 Å, *b* = 118.2 Å, *c* = 140.2 Å, α = 89.8°, *β* = 89.6°, *γ* = 76.5°	*a* = 75.9 Å, *b* = 119.0 Å, *c* = 141.4 Å, α = 89.9°, *β* = 89.9°, *γ* = 76.4°	*a* = 70.3 Å, *b* = 168.9 Å, *c* = 149.1 Å, *β* = 92.2°
maximal resolution (Å)	2.4	2.6	3.0
no. of measured reflections	277916	301890	142852
no. of unique reflections	161833	144679	68562
completeness (%)	87.6 (89.9)[a]	97.9 (97.4)[a]	98.7 (98.4)[a]
R_{merge}	0.058 (0.246)[a]	0.108 (0.505)[a]	0.089 (0.399)[a]
mean $I/\sigma I$	10.2 (3.0)[a]	8.0 (1.8)[a]	9.5 (1.7)[a]
Refinement			
resolution range (Å)	40−2.4	40−2.6	40−3.0
R_{work}/R_{free}[b]	0.199/0.253	0.193/0.250	0.240/0.297
average *B* factor (Å^2)			
proteins	27.6	34.8	67.4
waters	19.5	20.9	36.2
L-Asp	−	43.3	−
composition of asymmetric unit	8 polypeptide chains (residues ∼5−466, 3697 residues), 4 Ca^{2+}, 888 waters	8 polypeptide chains (residues ∼5−466, 3683 residues), 4 Ca^{2+}, 2 L-Asp, 479 waters	8 polypeptide chains (residues ∼5−394, 3108 residues) 2 Ca^{2+}, 60 waters
geometry			
rmsd for bonds (Å)	0.010	0.009	0.008
rmsd for angles (deg)	1.2	1.2	1.0
Ramachandran favored (%)	99.2	99.2	98.8
Ramachandran outliers (%)	0	0	0
Molprobity score	2.06	2.18	2.49
PDB entry	3R6Q	3R6V	3R6Y

[a] Data in parentheses are for the highest-resolution shell. [b] $R_{work} = \Sigma_{hkl}||F_o| - |F_c||/\Sigma_{hkl}|F_o|$, where the crystallographic R_{factor} was calculated with 95% of the data used in the refinement. R_{free} is the crystallographic R_{factor} based on 5% of the data withheld from the refinement for cross validation.

monitoring the increase in absorbance at 240 nm corresponding to the formation of fumarate (ε = 2530 M^{-1} cm^{-1}) as previously described.[22,23] Each kinetic assay was conducted twice, and the differences in k_{cat} and k_{cat}/K_m values were less than 25%.

Determination of the Structures of AspB and the AspB−L-Asp Complex (AspB−L-Asp). Attempts to crystallize AspB under previously reported conditions[21] were unsuccessful. Therefore, a search for new crystallization conditions was performed by sparse-matrix sampling using various commercially available crystallization kits. Screening was performed at room temperature in 96-well sitting-drop crystallization plates using a Mosquito (TTP LabTech) robot for drop dispensing. An initial crystallization hit was obtained with the JCSG+ (Qiagen) crystallization screen, which was optimized manually by using the hanging-drop vapor diffusion method, varying the precipitant concentration, pH, and temperature, and testing the effect of additives. Droplets were composed of 1 μL of an AspB protein stock solution and 1 μL of crystallization solution and were equilibrated against 500 μL of crystallization solution. The final crystallization solution contained 0.25 M NaSCN, 10 mM $CaCl_2$, 0.1 M HEPES (pH 7.0), and 20% PEG3350. Crystals grew at 4 °C within 2 days as single plates with maximal dimensions of 100 μm × 100 μm × 5 μm.

Prior to diffraction data collection, a single crystal was transferred into crystal mother liquor containing 12% PEG400 as a cryoprotectant. Mounted in a nylon loop, the crystal was subsequently dipped into liquid nitrogen. The substrate-bound state was trapped by soaking an AspB crystal for a few seconds in cryoprotectant solution supplemented with 100 mM L-aspartate, followed by immediate flash-cooling in liquid nitrogen. All these procedures were conducted at 4 °C. Diffraction data for unliganded AspB and AspB−L-Asp were collected at 100 K on single crystals on beamline ID14-1 of the ESRF (Grenoble, France) using an ADSC Quantum Q210 detector. The two data sets were indexed and integrated with XDS[26] and scaled using SCALA[27] from the CCP4 package (http://www.ccp4.ac.uk). Data collection statistics are listed in Table 1.

The unliganded triclinic structure of AspB was determined by molecular replacement using MOLREP.[28] A single subunit from the orthorhombic AspB structure [Protein Data Bank (PDB) entry 1J3U, chain A][21] was used as a search model. The presence of two independent tetramers in the P1 unit cell was verified by analysis of self-rotation Patterson maps and calculation of the Matthews coefficient (solvent content of 58%). The protein structure was optimized by restrained refinement using REFMAC5,[29] alternated with manual model building using Coot.[30]

At the final stages of refinement, water molecules were added to the model on the basis of strict geometrical and electron density criteria. For AspB−L-Asp, an initial map calculated with phases derived from the unliganded triclinic structure of AspB showed poor density for the SS loops of chains D and H. Manual rebuilding of the loop regions, followed by restrained refinement using REFMAC5, improved the electron density. Several additional cycles of manual model building and refinement, including the placement of water molecules into the structure, were conducted prior to the addition of L-aspartate to the model. Each tetramer had an L-aspartate molecule bound in one of its active site pockets, as revealed by inspection of $2F_o - F_c$ and $F_o - F_c$ Fourier maps (Figure S1 of the Supporting Information). The final refinement statistics for both structures are listed in Table 1.

Limited Proteolysis of AspB. α-Chymotrypsin (Sigma, stock solution, 1 mg/mL in 1 mM HCl and 1 mM $CaCl_2$) was added to purified AspB [in 25 mM Tris buffer (pH 7.5) at ∼6.8 mg/mL] at a 1:1000 (w/w) ratio. The mixture was incubated at room temperature for 2 days, and the proteolysis reaction was stopped by addition of PMSF to a final concentration of 1 mM. The proteolytic cleavage was followed by SDS−PAGE, revealing the production of an ∼44 kDa stable proteolytic fragment. Without additional purification, the chymotrypsin-treated protein was used for crystallization, mass spectrometry, and activity analysis. For MALDI-TOF mass spectrometry, the fragment was mixed in a 1:1 (v/v) ratio with a solution of α-cyano-4-hydroxycinnamic acid (10 mg/mL in 70% acetonitrile and 0.1% trifluoroacetic acid), spotted onto a stainless steel MALDI target, and analyzed on a model 4800 Proteomics analyzer (AB SCIEX) in the linear mode following standard procedures. The mass of the intact chymotrypsin-cleaved AspB fragment was determined to be 44231 ± 12 Da, which matches the calculated mass of an AspB fragment comprising residues 1−401 (44235 Da).

Determination of the Structure of Chymotrypsin-Treated AspB. Chymotrypsin-treated AspB (chymo-AspB) was crystallized by using the hanging-drop vapor diffusion method. The protein solution was mixed with crystallization solution that contained 0.2 M calcium acetate, 0.1 M HEPES (pH 7.5), and 40% PEG400. Thick elongated platelike crystals appeared in a few days and grew to a maximal size of 60 μm × 300 μm × 10 μm in ∼1 week. For data collection, crystals were mounted in a nylon loop and frozen directly in liquid nitrogen. Diffraction data extending to 3.0 Å resolution were collected from a frozen crystal on beamline ID14-2 at ESRF, equipped with an ADSC Quantum 4 detector. The data set was indexed and integrated using Mosflm[31] and scaled using SCALA from the CCP4 package (see Table 1 for data collection and proccesing statistics).

The structure of chymo-AspB (space group *P*1, eight molecules per asymmetric unit) was determined by molecular replacement with MOLREP. The unliganded AspB structure, with residues 402−466 removed, was used as search model. The obtained solution was initially refined by applying rigid-body and NCS-restrained refinement in REFMAC5. The model was completed by several rounds of restrained refinement using REFMAC5, interspersed with manual model building using COOT. Model refinement statistics are listed in Table 1.

Structure Analysis. Structure validation was performed with Molprobity.[32] Structure superpositions and calculation of rmsds were conducted using Superpose.[33]

Figures. Figures were prepared using PyMOL (http://pymol.sourceforge.net).

RESULTS

Determination of the Structures of Unliganded and L-Asp-Bound AspB. AspB was crystallized in a ligand-free state under different conditions and in a crystal form different from that reported previously.[21] Crystals belong to space group *P*1 and contain two physiologically relevant tetramers per unit cell. The triclinic structure of AspB was determined at 2.4 Å resolution by molecular replacement, using the previously reported orthorhombic structure as a search model, and refined to an R_{free} of 25.3% and an R_{factor} of 19.9%. The L-aspartate-bound state of AspB was captured by performing a quick soak of the triclinic crystals in 100 mM L-aspartate (L-Asp) at 277 K, immediately followed by flash-cooling in liquid nitrogen. Inspection of $F_o - F_c$ difference electron density maps revealed that in each of the two tetramers in the unit cell one of the four active sites contained an L-Asp molecule. The structure of L-Asp-bound AspB was determined and refined at 2.6 Å resolution to an R_{free} of 25.0% and an R_{factor} of 19.3% (see Table 1 for a summary of the relevant crystallographic statistics). The subunits in the refined apo-AspB and AspB−L-Asp structures all contain 462 residues as there was insufficient electron density present to model residues 1−4, 467, and 468 in each monomer. The overall structures of the two crystallographically independent tetramers in the unit cell are identical [the pairwise Cα backbone root-mean-square deviations (rmsd) are 0.07 and 0.11 Å for the two unliganded and L-Asp-bound AspB tetramers, respectively], as are the overall binding modes of the two aspartate molecules. For the sake of clarity, we will therefore mostly restrict our description and analysis to a single tetramer.

Overall Structure and Substrate-Induced Conformational Changes. The unliganded AspB structure determined in this study is identical to that reported previously by Fujii et al.[21] Briefly, AspB exists as a homotetramer with 222 point symmetry (Figure 1). Each of the subunits has approximate dimensions of 40 Å × 50 Å × 100 Å and is composed of three structurally distinct domains: the so-called "N-terminal large domain" (residues 5−139), containing a two-stranded antiparallel β-hairpin followed by five α-helices; the "central helix domain" (residues 140−393), mainly containing six long antiparallel α-helices; and the "C-terminal small domain" (residues 394−466), which consists of seven small α-helices. In the tetramer, the central helix domain of each subunit interacts coaxially with those of the other three subunits to form a well-packed bundle of 20 α-helices. The N- and C-terminal domains of adjacent subunits meet at the ends of this helical bundle, forming four beaklike protrusions. Inside these protrusions are the four independent active sites of the AspB tetramer. Each active site is located in a pocket formed by two conserved N-terminal segments (residues 96−110 and 135−143) and a central domain segment (residues 183−194) of two adjacent subunits (for a representative active site, we will refer to these subunits as A and B) that is complemented by a nearby SS loop (residues 317−328) from a third subunit (subunit C). In the unliganded AspB tetramer, each SS loop interacts with the C-terminal domain of a neighboring subunit (e.g., the SS loop of subunit C interacts with the C-terminal domain of subunit A), locking it in an open conformation away from the active site pocket. However, with substrate present in the active site, as observed in the L-Asp-bound AspB tetramer, the SS loop adopts a dramatically different conformation, in which it no longer contacts the C-terminal domain but instead closes over the active site allowing it to

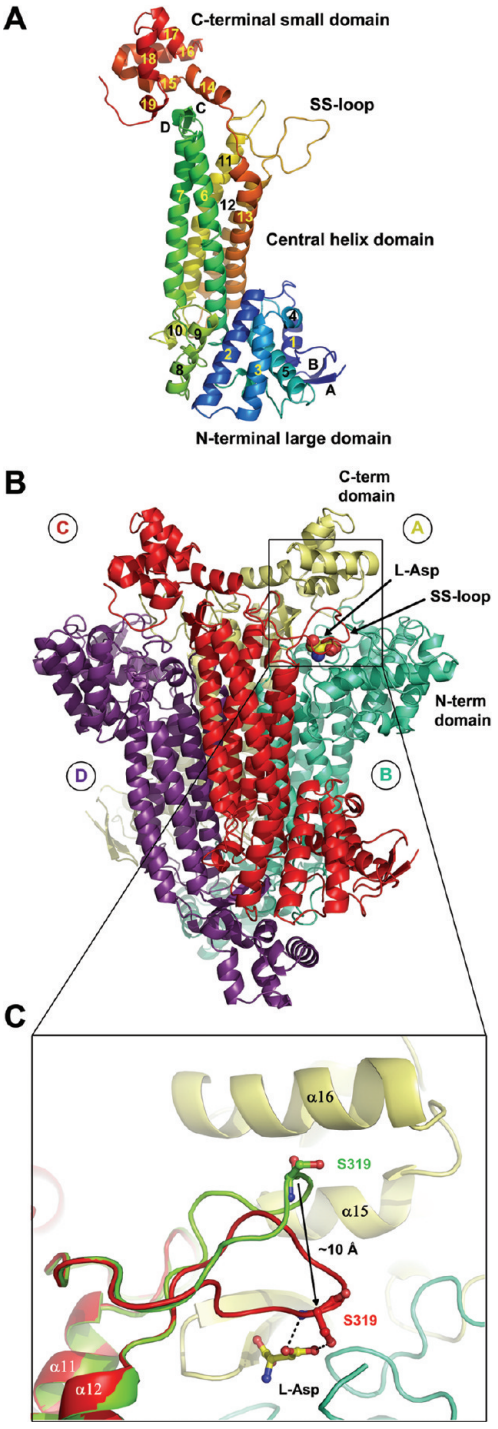

Figure 1. Overall structure of AspB. (A) Ribbon representation of an AspB subunit with a rainbow color gradient from the N-terminus (blue) to the C-terminus (red). Secondary structure elements are indicated with numbers for α-helices and letters for β-strands. (B) Ribbon representation of the L-Asp-bound AspB tetramer. Subunits A−D are labeled and are colored pale yellow, cyan, red, and purple, respectively. The bound L-Asp is drawn as a CPK model, with its carbon, nitrogen, and oxygen atoms colored yellow, blue, and red, respectively. (C) Superposition of the SS loops at the ABC active site in the unliganded and L-Asp-bound AspB structures, showing the open-to-closed conformational change (green, unliganded, open conformation; red, liganded, closed conformation). Hydrogen bonds between Ser319 and L-Asp are depicted as dashed lines.

participate in substrate binding. The closed and open Cα backbone conformations of the SS loop have an rmsd of ~6 Å with Ser319 showing the largest displacement of ~10 Å (Figure 1C).

As mentioned above, only one of the active sites in the tetramer of the AspB−L-Asp structure has a substrate bound (for the sake of convenience, we have labeled this as the ABC active site, referring to its participating subunits). In the crystal, the ABC active site (and the equivalent EFG active site of the other, crystallographically independent tetramer) is adjacent to a solvent channel and not making any crystal packing contacts. In contrast, the other active sites are in areas where the tetramers make multiple crystal contacts, thereby restricting their conformational flexibility. Interestingly, the substrate-induced conformational change of the SS loop at the ABC active site coincides with a significant increase in the overall temperature factor of the C-terminal domain in subunit A, which changes from ~57 Å^2 in the unliganded AspB structure to ~95 Å^2 in the AspB−L-Asp complex [the other C-terminal domains in the tetramer show a similar *B* factor of ~40 Å^2 in both structures (see Figure S2 of the Supporting Information)]. A similar effect is observed for the other tetramer present in the crystal. The higher mobility of the C-terminal domain at the substrate-bound active site is also apparent from the significantly weaker electron density associated with this domain, as compared to the C-terminal domains that are adjacent to the unliganded active sites. Apparently, in the open conformation, the SS loop stabilizes the adjacent C-terminal domain, which becomes highly mobile when this loop detaches upon substrate binding. Apart from the conformational change in the SS loop, and the increase in the mobility of the adjacent C-terminal domain, no significant changes are observed in the AspB structure upon substrate binding.

L-Asp Is Bound in a High-Energy, Enediolate-like Conformation. The bound L-Asp substrate in the active site of AspB is stabilized by an extensive number of interactions (Figure 2), most of which have previously been predicted on the basis of modeling and mutagenesis studies.[21,23] Interestingly, and not noted previously, the substrate binding interactions force the side chain of the bound L-Asp to adopt an energetically unfavorable rotamer in which the Cα, Cβ, and β-carboxylic atoms are almost coplanar, thus resembling the conformation of the putative enediolate intermediate in catalysis. As explained above, the residues of AspB that bind the substrate originate from three different subunits and are part of four conserved regions: residues 96−110 and 135−143 from subunit B, residues 183−194 from subunit A, and residues 317−328 (the SS loop) from subunit C. The α-amino group of L-Asp is hydrogen bonded to the side chains of Thr101, Asn142, and His188, while the α-carboxylate group forms hydrogen bonds with the side chains of Asn142, Thr187, and Lys324. The positively charged side chain of Lys324 further stabilizes the negative charge on the α-carboxylate group by an electrostatic interaction, which is crucial for the functioning of AspB as shown previously by site-directed mutagenesis.[23] The oxygens of the β-carboxylate group of L-Asp (Oδ1 and Oδ2) are within hydrogen bonding distance of four side chain hydroxyl groups and two main chain amides of AspB (Thr101, Ser140, Thr141, and Ser319). However, considering that in its ground state the Oδ1 and Oδ2 atoms of aspartate are sp^2 hybridized, some of the potential hydrogen bonds exhibit an unfavorable geometry. All hydrogen bonds would be appropriate, though, for stabilizing a high-energy conformation of the side chain in which the Oδ1 and Oδ2 atoms are sp^3 hybridized, consistent with a polarization of the β-carboxylate C−O bonds that is expected to

dx.doi.org/10.1021/bi200497y |*Biochemistry* 2011, 50, 6053–6062

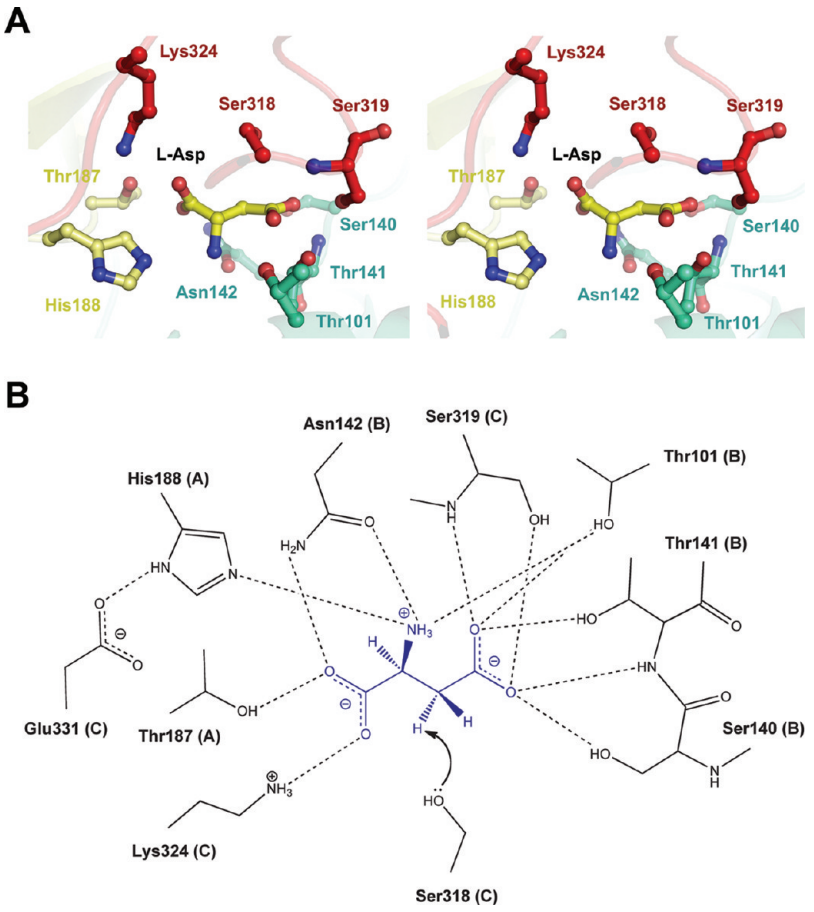

Figure 2. L-Asp binding mode. (A) Stereoview of the AspB active site with bound L-Asp (yellow) showing the residues that form hydrogen bonds with the substrate. The coloring scheme is the same as in Figure 1. (B) Schematic representation of the interactions between L-Asp and AspB. Hydrogen bonds are represented as dashed lines. The putative role of Ser318 as a catalytic base, abstracting the *pro-R* hydrogen from the Cβ atom of the substrate, is depicted with an arrow.

occur in the enediolate-like transition state and enediolate intermediate.[18,20,23] Hence, in addition to its role in substrate binding, this extensive hydrogen bonding network with the β-carboxylate group appears to be important for stabilizing the additional negative charge that develops on one of the carboxylate oxygens upon abstraction of a proton. Notably, there is no nearby positively charged residue to assist in the stabilization of the negatively charged β-carboxylate group. However, as suggested previously on the basis of substrate- and product-bound structures of *E. coli* adenylosuccinate lyase,[3] the negative charge(s) on the β-carboxylate group of the substrate or enediolate intermediate may be further stabilized by an electrostatic interaction with the dipole moment of helix α6 (Figure 3A).

The AspB—L-Asp structure further provides clear evidence that the SS loop contributes significantly to substrate binding. In addition to the interactions of Ser319 and Lys324 with the two carboxylate groups of the substrate mentioned above, the carbonyl oxygen of Gly317 and the side chain of Ser318 make van der Waals contacts with the Cα and Cβ atoms of L-Asp. Noteworthy is the fact that the Oγ atom of Ser318 is positioned only 3.6 Å from the Cβ atom of L-Asp and at an angle that would be suitable for abstracting the Cβ *pro-R* proton.

Structural Comparison with Other Members of the Aspartase/Fumarase Superfamily. The biological significance of the AspB—L-Asp structure was further analyzed by comparing it to the structure of the His171Ala mutant of *E. coli* adenylosuccinate lyase with bound adenylosuccinate (*ec*ADL-H171A—ADS),[3] one of the few members of the aspartase/fumarase superfamily for which a structure of its complex with uncleaved natural substrate has been reported. This comparison revealed that in one of the two crystallographically independent substrate molecules in the *ec*ADL-H171A—ADS crystal, the succinyl moiety has an enediolate-like conformation similar to that of the bound L-Asp molecules in the AspB crystal (Figure 3A). The second bound adenylosuccinate (ADS) molecule in *ec*ADL-H171A—ADS exhibits a low-energy rotamer conformation of its succinyl moiety, but the adjacent SS loop is highly disordered and does not show a closed conformation, suggesting that the observed binding mode of this substrate molecule is less tight and probably nonproductive. For the formerly mentioned ADS molecule, the binding mode of its succinyl moiety in the active site of *ec*ADL-H171A is highly similar to that of L-Asp in AspB, with the two carboxylate groups forming an almost identical hydrogen bonding network with residues His91, Thr122, Ser123, Thr170, Ser296, and Lys301 (the equivalents of Thr101, Ser140, Thr141, Thr187, Ser319, and Lys324, respectively, in AspB). Moreover, the SS loop adjacent to the bound substrate in *ec*ADL-H171A adopts a closed conformation, like the SS loop in the L-Asp-bound active site of AspB, with Ser295 (the equivalent of Ser318 in AspB) positioned close to the Cβ atom of the succinyl

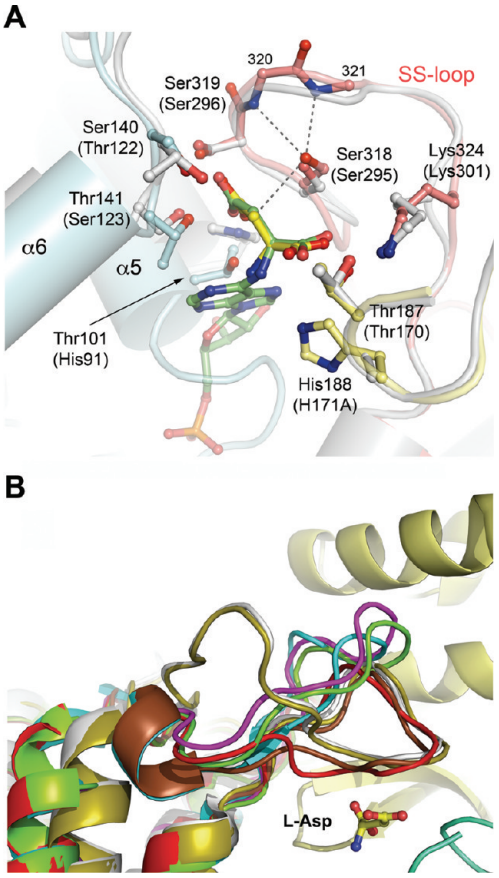

Figure 3. Structural comparison of AspB with other members of the aspartase/fumarase superfamily. (A) Overlay of the active sites of AspB—L-Asp (coloring scheme as in Figure 1, with L-Asp colored yellow) and *ec*ADL-H171A—ADS (gray, with ADS colored green), showing the conserved binding mode of the common succinyl moieties. Residue labels of *ec*ADL are given in parentheses. Dashed lines indicate the interactions of Ser318 with the amide backbones of Ile320 and Met321, and with the Cβ atom of L-AspB. (B) Comparison of SS loop conformations in structures of different members of the aspartase/fumarase superfamily, i.e., unliganded AspB (light-green), L-Asp-bound AspB (red), citrate-bound fumarase C from *E. coli* (PDB entry 1FUO, magenta),[10] unliganded duck δ2-crystallin (PDB entry 1HY1, cyan),[2] ADS-bound *ec*ADL-H171A (PDB entry 2PTR, gray),[3] *ec*ADL-H171N bound to AMP and fumarate (PDB entry 2PTQ, light brown),[3] and duck δ1-crystallin bound to sulfate ion (PDB entry 1HY0, dark brown).[2]

moiety. It thus appears that the key features of the substrate binding mode in AspB—L-Asp, i.e., an extensive hydrogen bonding network to stabilize and polarize the substrate's β-carboxylate group, closure of the SS loop, and the positioning of one of the conserved SS loop serine residues close to the substrate's Cβ atom, are all conserved in *ec*ADL-H171A—ADS, emphasizing the close relationship between AspB and *ec*ADL.

Conformational Flexibility of the SS Loop and Its Importance for Activity. These AspB structures reveal a large conformational change in the SS loop from an open conformation in the absence of substrate to one that closes over the active site in the presence of substrate. The closed conformation of the SS loop in AspB—L-Asp is similar to that observed in the structures of *ec*ADL and duck δ1-crystallin with bound substrate, product, or substrate mimics (Figure 3B). The open conformation of the SS loop in the absence of bound substrate is similar to that in the previously reported unliganded structures of AspB, duck δ2-crystallin, and citrate-bound *E. coli* fumarase C. In the unliganded structures of other members of the aspartase/fumarase superfamily, including *E. coli* AspA, the SS loop is highly disordered. In contrast, in our AspB structures, the SS loops associated with the empty active sites are relatively ordered and adopt the same open conformation, as shown by an average pairwise backbone rmsd of 0.7 Å^2 (calculated for residues 317—324). The open conformation of the SS loop is stabilized by hydrophobic contacts of the side chains of Ile320 and Met321 with a hydrophobic surface patch on the adjacent C-terminal domain [formed by residues Ile406, Ile409, Tyr418, Ala421, Ala422, Ala425, and Tyr429 (Figure 4)].

The functional importance of the interactions of the SS loop in the open and closed conformations was studied by creating five single site-directed mutations, i.e., Ser318Ala, Ser319Ala, Ile320Ala, Met321Ala, and Pro322Ala. Each mutant was purified to homogeneity and analyzed for its deamination activity toward L-aspartic acid (Table 2). The Ser319Ala mutant, like the Pro322Ala mutant, shows kinetic parameters similar to those of wild-type AspB, indicating that the contribution of the conserved Ser319 residue to the hydrogen bonding network with the β-carboxylate group of L-Asp is not that significant. In contrast, mutation of Ser318 to an alanine causes a complete inactivation of the enzyme, consistent with a direct role of this residue in AspB catalysis, most likely as the general base catalyst, which has been proposed for Ser295 in *ec*ADL.[3] Surprisingly, for the Ile320Ala and Met321Ala mutants also, a large decrease in catalytic efficiency was observed, primarily due to a large increase in K_m values. In the closed conformation of the SS loop, residues Ile320 and Met321 point away from the active site and are largely solvent exposed; thus, one would not expect such a large decrease in activity and substrate binding affinity upon mutation. However, the mutation of Ile320 or Met321 to an alanine residue may destabilize the open conformation of the SS loop by disrupting the interaction with the C-terminal domain. We therefore suggest that the decreased catalytic efficiency of these AspB mutants may be caused by an increased level of disorder in the SS loop, thereby preventing efficient loop closure, which, in turn, may affect substrate binding and positioning.

Proteolytic Removal of the C-Terminal Domain Inactivates AspB. The highly reduced catalytic efficiency of the Ile320Ala and Met321Ala mutants suggests that the interactions between the open SS loop and the C-terminal domain of AspB are important for its enzymatic function. To provide further evidence to support this hypothesis, we subjected AspB to limited proteolysis, aiming at the full or partial deletion of the C-terminal domain. Using α-chymotrypsin, it was possible to generate a stable proteolytic fragment of AspB, which remained tetrameric but showed a subunit size of 44 kDa (as judged from SDS—PAGE and gel filtration), consistent with the absence of the C-terminal domain (Figure S3 of the Supporting Information). Further analysis of chymotrypsin-treated AspB (hereafter named chymo-AspB) by mass spectrometry revealed that cleavage had occurred after residue Tyr401, which is located within a surface-exposed helix (α14) at the beginning of the C-terminal domain. Kinetic analysis showed that chymo-AspB exhibits no detectable activity toward L-Asp (data not shown).

To identify the effects of removing the C-terminal domain on the rest of the AspB structure, we crystallized chymo-AspB and determined and refined its crystal structure at 3.0 Å resolution to an R_{free} of 24.0% and an R_{factor} of 29.7% (Table 1). Other than

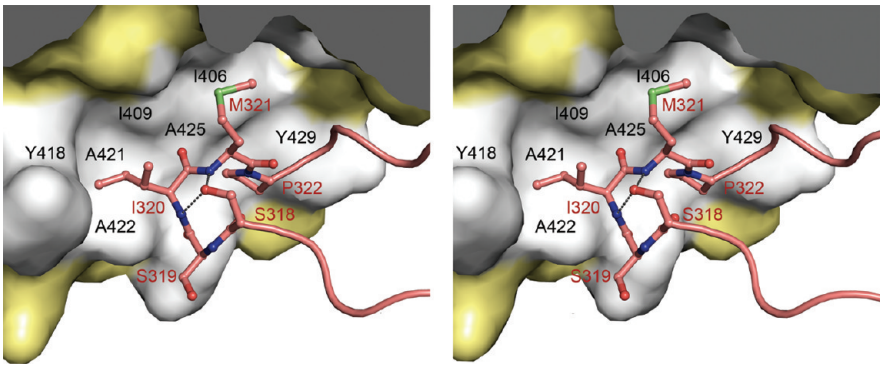

Figure 4. Stabilization of the open SS loop conformation. Stereoview of the open SS loop (red, subunit C, ribbon representation) and its contacts with the C-terminal domain (yellow, subunit A, surface representation) in the unliganded AspB structure. Subunit B is not shown for the sake of clarity. The side chains of Ile320, Met321, and Pro322 in the SS loop are shown in ball-and-stick representations. The hydrophobic residues of the C-terminal domain of subunit A that contact these three SS loop residues are colored gray and identified with black labels. Also shown are Ser318 and Ser319. Dashed lines indicate the interactions of Ser318 with the amide backbones of Ile320 and Met321.

Table 2. Kinetic Parameters for the Deamination of L-Aspartic Acid by Wild-Type AspB-His and the SS Loop Mutants

enzyme	K_m (mM)	k_{cat} (s^{-1})	k_{cat}/K_m (M^{-1} s^{-1})
wild type[a]	15 ± 2	40 ± 7	2.7×10^3
S318A	–	–	$<10^{-3}$
S319A	28 ± 4	17 ± 1	6.1×10^2
I320A	>100	–	5.5×10
M321A	>100	–	0.8×10
P322A	11 ± 1	21 ± 0.5	1.9×10^3

[a] The kinetic data were obtained from ref 23. Errors are standard deviations from each fit.

the absence of the C-terminal domains, no significant overall structural differences were observed in the chymo-AspB tetramer compared to the unliganded, full-length AspB tetramer (the average tetrameric Cα backbone rmsd is 0.4 Å for four times 382 common residues, excluding the SS loops). Near the active site, the only local conformational consequence of removing the C-terminal domain concerns the SS loop. In two of the subunits of the chymo-AspB tetramer, poor electron density is observed for the SS loop, indicative of a high degree of disorder. In the other two subunits, the SS loop adopts a defined conformation, but that conformation is stabilized by crystal contacts of residues Ile320, Met321, and Pro322 with residues of a neighboring tetramer and differs from the open or closed conformation in the full-length AspB structures. Thus, it seems that, as for the Ile320Ala and Met321Ala mutants, the negative effect on AspB activity upon removal of the C-terminal domain is related to a disruption of the SS loop−C-terminal domain interactions, resulting in an increased level of disorder of the SS loop.

■ DISCUSSION

The structure of the AspB−L-Asp complex determined in this study provides strong experimental support for the proposal that conversion of L-Asp to fumarate and ammonia proceeds via general base-catalyzed formation of an enzyme-stabilized enediolate intermediate (Figure 5). The highly structured active site environment, the observed high-energy conformation of the bound substrate, the closed SS loop conformation, and the extensive hydrogen bonding network with the substrate's β-carboxylate group show how the active site of AspB is primed for stabilizing an enediolate-like transition state and enediolate intermediate.

Our results further reveal that the SS loop serves a crucial role in the catalytic mechanism of AspB. Its closure over the active site provides additional substrate binding stabilization and ensures that the substrate is sequestered from the solvent during catalysis. A similar closure of the SS loop has been observed in the crystal structures of *ec*ADL with bound substrate or product, and duck δ1-crystallin with bound sulfate.[2,3] However, more often the SS loop is found to be disordered or in an open conformation in structures of other members of the aspartase/fumarase superfamily, even in the presence of substrate in the active site.[5,8,10] Closure of the SS loop is thus not dependent on only the presence of a succinyl moiety (or other ligand) in the enzyme active site. In fact, as shown in this study for AspB, the C-terminal domain may play a crucial role in controlling the conformational change of the SS loop, and thus in regulating enzyme activity. Hence, the factors that govern closure of the SS loop are highly complex. Most importantly, we observed that closure of the SS loop positions Ser318 near the Cβ proton of L-Asp, in a suitable orientation to allow proton abstraction in the first step of the reaction. Although the involvement of serine as a catalytic base is highly unusual given its intrinsically high pK_a value, such a role for Ser318 in AspB is supported by several additional observations. First, the participation of a basic group in AspB catalysis has been revealed by kinetic studies,[23] and there are no AspB residues other than Ser318 in the vicinity of the Cβ atom of L-Asp that could act as a catalytic base. Second, the complete lack of activity of the Ser318Ala mutant and the strict conservation of this residue across all members of the aspartase/fumarase superfamily strongly indicate that Ser318 has an essential role in AspB catalysis. Finally, a role as a catalytic base has also been proposed for the SS loop Ser295 of *ec*ADL,[3] and the structural comparison of AspB−L-Asp and substrate-bound *ec*ADL shows that Ser318 of AspB and Ser295 of *E. coli* ADL are structurally and functionally equivalent.

The question of how Ser318 is activated to function as a catalytic base remains. A possible mechanism would be the deprotonation of Ser318 by a neighboring base to form a Ser-O^- oxyanion, which then abstracts the Cβ proton of L-Asp. Such

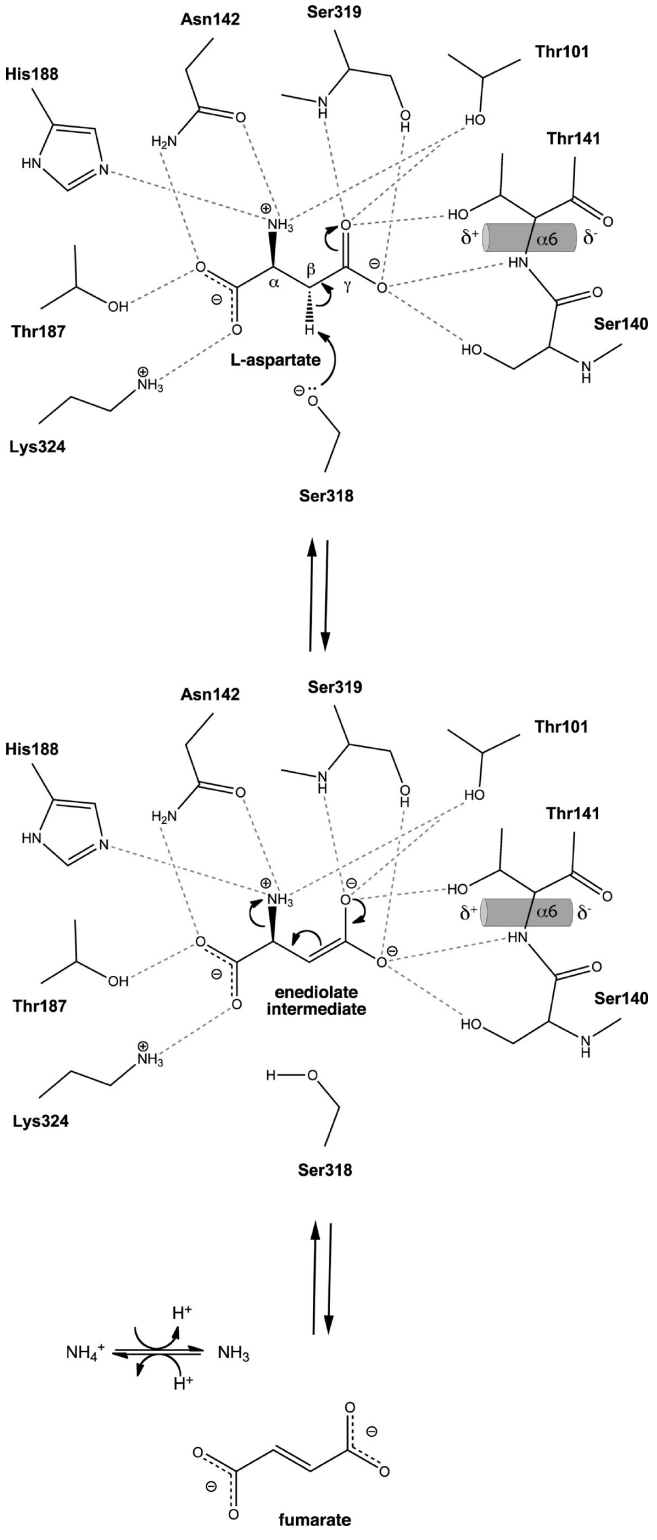

Figure 5. Schematic representation of the proposed catalytic mechanism of AspB.

a mechanism, however, requires a substantial perturbation of the pK_a of Ser318 by its microenvironment in the substrate-bound active site (the predicted intrinsic pK_a of the serine-OH group is 15). Stabilization of the serine oxyanion (and resulting decrease in the pK_a value of the Ser-OH species) may be realized due to interactions with the backbone amides of Ile320 and Met321 (Figure 3A), similar to what has been proposed for Ser295 in *ec*ADL.[3] Furthermore, a role of the substrate in activating the SS loop serine could be considered, with the β-carboxylate group acting as a base to generate the serine oxyanion, which has been proposed for *Plasmodium falciparum* adenylosuccinate lyase.[34] In pH profiles (pH 5.8−8.8) of this lyase, the group corresponding to the catalytic base becomes ionized in the enzyme−substrate complex but not in the free enzyme. This suggests that in the reaction catalyzed by *P. falciparum* adenylosuccinate lyase the substrate (succinyl-adenosine monophosphate) assists in the ionization of the catalytic base. However, in the case of AspB, previous kinetic studies revealed that the group corresponding to the catalytic base is already ionized in the substrate-free enzyme (pK_a ∼ 7.1), and its pK_a value undergoes only a relatively small extra decrease in the enzyme−substrate complex (pK_a ∼ 6.2).[23] In the open SS loop conformation, Ser318 of AspB forms similar interactions with the amides of Ile320 and Met321 as in the closed SS loop conformation (Figure 4), suggesting that these interactions are the main contributors to the serine oxyanion stabilization. An additional contribution from the substrate cannot be excluded, though. Given the large displacement of Ser318 upon substrate binding, the already perturbed pK_a of the catalytic base in the free enzyme may obscure the effect of L-Asp on ionization of the catalytic base when positioned in the active site upon closure of the SS loop. Hence, these data do not allow us to determine the exact mechanism of activation of Ser318 as a catalytic base and whether the substrate assists in ionizing the catalytic serine residue.

In conclusion, the high-resolution structure of the AspB−L-Asp complex described herein provides the first detailed view of the substrate-bound active site of an aspartase, allowing an improved understanding of the roles of the various active site residues in substrate binding and catalysis. Our results further give credence to the notion that all aspartase/fumarase superfamily members use a common catalytic mechanism, which involves general base-catalyzed formation of an enzyme-stabilized enediolate intermediate and the participation of the SS loop in substrate binding and catalysis.

■ ASSOCIATED CONTENT

Supporting Information. Additional figures showing electron density maps of the SS loop (open and closed conformations) and of bound L-asparate, residue-averaged temperature factor distribution in the unliganded AspB and AspB−L-Asp structures, and SDS−PAGE analysis and crystal packing arrangement of chymotrypsin-treated AspB. This material is available free of charge via the Internet at http://pubs.acs.org.

■ AUTHOR INFORMATION

Corresponding Author

*A.-M.W.H.T.: Department of Biophysical Chemistry, Groningen Biomolecular Sciences and Biotechnology Institute, University of Groningen, Nijenborgh 7, 9747 AG Groningen, The Netherlands; phone, +31 50 363-4380; fax, +31 50 363-4800; e-mail, a.m.w.h.thunnissen@rug.nl. G.J.P.: Department of Pharmaceutical Biology, Groningen Research Institute of Pharmacy, University of Groningen, Antonius Deusinglaan 1, 9713 AV Groningen, The Netherlands; phone, +31 50 363-3354; fax, +31 50 363-3000; e-mail, g.j.poelarends@rug.nl.

Funding Sources

This research was supported in part by an Ubbo Emmius Bursary (University of Groningen) awarded to G.F. G.J.P. was supported by VENI and VIDI grants from the Division of Chemical Sciences of The Netherlands Organisation of Scientific Research (NWO-CW).

■ ACKNOWLEDGMENT

We thank Fabrizia Fusetti for assistance with mass spectrometry and Bauke Dijkstra for critical reading of the manuscript. We also thank the ESRF staff at the MX beamlines for assistance.

■ ABBREVIATIONS

AspA, *E. coli* aspartase; AspB, aspartase from *Bacillus* sp. YM55-1; *ec*ADL, *E. coli* adenylosuccinate lyase; ADS, adenylosuccinate; rmsd, root-mean-square deviation.

■ REFERENCES

(1) Mizobata, T., and Kawata, Y. (2007) Aspartases: Molecular structure, biochemical function and biotechnological applications. In *Industrial Enzymes: Structure, function and applications* (Polaina, J., and MacCabe, A. P., Eds.) pp 549−565, Springer, New York.

(2) Sampaleanu, L. M., Vallçe, F., Slingsby, C., and Howell, P. L. (2001) Structural studies of duck δ1 and δ2 crystallin suggest conformational changes occur during catalysis. *Biochemistry 40*, 2732–2742.

(3) Tsai, M., Koo, J., Yip, P., Colman, R. F., Segall, M. L., and Howell, P. L. (2007) Substrate and product complexes of *Escherichia coli* adenylosuccinate lyase provide new insights into the enzymatic mechanism. *J. Mol. Biol. 370*, 541–554.

(4) Turner, M. A., Simpson, A., McInnes, R. R., and Howell, P. L. (1997) Human argininosuccinate lyase: A structural basis for intragenic complementation. *Proc. Natl. Acad. Sci. U.S.A. 94*, 9063–9068.

(5) Vallee, F., Turner, M. A., Lindley, P. L., and Howell, P. L. (1999) Crystal structure of an inactive duck δ II crystallin mutant with bound argininosuccinate. *Biochemistry 38*, 2425–2434.

(6) Weaver, T. M., Levitt, D. G., Donnelly, M. I., Stevens, P. P., and Banaszak, L. J. (1995) The multisubunit active site of fumarase C from *Escherichia coli*. *Nat. Struct. Biol. 2*, 654–662.

(7) Yang, J., Wang, Y., Woolridge, E. M., Arora, V., Petsko, G. A., Kozarich, J. W., and Ringe, D. (2004) Crystal structure of 3-carboxy-cis, cis-muconate lactonizing enzyme from *Pseudomonas putida*, a fumarase class II type cycloisomerase: Enzyme evolution in parallel pathways. *Biochemistry 43*, 10424–10434.

(8) Sampaleanu, L. M., Yu, B., and Howell, P. L. (2002) Mutational analysis of duck δ2 crystallin and the structure of an inactive mutant with bound substrate provide insight into the enzymatic mechanism of argininosuccinate lyase. *J. Biol. Chem. 277*, 4166–4175.

(9) Chakraborty, A. R., Davidson, A., and Howell, P. L. (1999) Mutational analysis of amino acid residues involved in argininosuccinate lyase activity in duck δ II crystallin. *Biochemistry 38*, 2435–2443.

(10) Weaver, T., and Banaszak, L. (1996) Crystallographic studies of the catalytic and a second site in fumarase C from *Escherichia coli*. *Biochemistry 35*, 13955–13965.

(11) Wu, C. Y., Lee, H. J., Wu, S. H., Chen, S. T., Chiou, S. H., and Chang, G. G. (1998) Chemical mechanism of the endogenous argininosuccinate lyase activity of duck lens δ2-crystallin. *Biochem. J. 333*, 327–334.

(12) Karsten, W. E., Hunsley, J. R., and Viola, R. E. (1985) Purification of aspartase and aspartokinase-homoserine dehydrogenase I from *Escherichia coli* by dye-ligand chromatography. *Anal. Biochem. 147*, 336–341.

(13) Kawata, Y., Tamura, K., Yano, S., Mizobata, T., Nagai, J., Esaki, N., Soda, K., Tokushige, M., and Yumoto, N. (1999) Purification and characterization of thermostable aspartase from *Bacillus* sp. YM55-1. *Arch. Biochem. Biophys. 366*, 40–46.

(14) Nuiry, I. I., Hermes, J. D., Weiss, P. M., Chen, C. Y., and Cook, P. F. (1984) Kinetic mechanism and location of rate-determining steps for aspartase from *Hafnia alvei*. *Biochemistry 23*, 5168–5175.

(15) Sun, D. X., and Setlow, P. (1991) Cloning, nucleotide sequence, and expression of the *Bacillus subtilis* ans operon, which codes for L-asparaginase and L-aspartase. *J. Bacteriol. 173*, 3831–3845.

(16) Suzuki, S., Yamaguchi, J., and Tokushige, M. (1973) Studies on aspartase. I. Purification and molecular properties of aspartase from *Escherichia coli*. *Biochim. Biophys. Acta 321*, 369–381.

(17) Takagi, J. S., Fukunaga, R., Tokushige, M., and Katsuki, H. (1984) Purification, crystallization, and molecular properties of aspartase from *Pseudomonas fluorescens*. *J. Biochem. 96*, 545–552.

(18) Yoon, M. Y., Thayer-Cook, K. A., Berdis, A. J., Karsten, W. E., Schnackerz, K. D., and Cook, P. F. (1995) Acid-base chemical mechanism of aspartase from *Hafnia alvei*. *Arch. Biochem. Biophys. 320*, 115–122.

(19) Shi, W., Dunbar, J., Jayasekera, M. M., Viola, R. E., and Farber, G. K. (1997) The structure of L-aspartate ammonia-lyase from *Escherichia coli*. *Biochemistry 36*, 9136–9144.

(20) Viola, R. E. (2000) L-Aspartase: New tricks from an old enzyme. *Adv. Enzymol. Relat. Areas Mol. Biol. 74*, 295–341.

(21) Fujii, T., Sakai, H., Kawata, Y., and Hata, Y. (2003) Crystal structure of thermostable aspartase from *Bacillus* sp. YM55-1: Structure-based exploration of functional sites in the aspartase family. *J. Mol. Biol. 328*, 635–654.

(22) Weiner, B., Poelarends, G. J., Janssen, D. B., and Feringa, B. L. (2008) Biocatalytic enantioselective synthesis of *N*-substituted aspartic acids by aspartate ammonia lyase. *Chem.—Eur. J. 14*, 10094–10100.

(23) Puthan Veetil, V., Raj, H., Quax, W. J., Janssen, D. B., and Poelarends, G. J. (2009) Site-directed mutagenesis, kinetic and inhibition studies of aspartate ammonia lyase from *Bacillus* sp. YM55-1. *FEBS J. 276*, 2994–3007.

(24) Kawata, Y., Tamura, K., Kawamura, M., Ikei, K., Mizobata, T., Nagai, J., Fujita, M., Yano, S., Tokushige, M., and Yumoto, N. (2000) Cloning and over-expression of thermostable *Bacillus* sp. YM55-1 aspartase and site-directed mutagenesis for probing a catalytic residue. *Eur. J. Biochem. 267*, 1847–1857.

(25) Ho, S. N., Hunt, H. D., Horton, R. M., Pullen, J. K., and Pease, L. R. (1989) Site-directed mutagenesis by overlap extension using the polymerase chain reaction. *Gene 77*, 51–59.

(26) Kabsch, W. (1993) Automatic processing of rotation diffraction data from crystals of initially unknown symmetry and cell constants. *J. Appl. Crystallogr. 26*, 795–800.

(27) Evans, P. (2006) Scaling and assessment of data quality. *Acta Crystallogr. D62*, 72–82.

(28) Vagin, A., and Teplyakov, A. (1997) MOLREP: An automated program for molecular replacement. *J. Appl. Crystallogr. 30*, 1022–1025.

(29) Murshudov, G. N., Vagin, A. A., and Dodson, E. J. (1997) Refinement of macromolecular structures by the maximum-likelihood method. *Acta Crystallogr. D53*, 240–255.

(30) Emsley, P., Lohkamp, B., Scott, W. G., and Cowtan, K. (2010) Features and development of Coot. *Acta Crystallogr. D66*, 486–501.

(31) Leslie, A. G. (2006) The integration of macromolecular diffraction data. *Acta Crystallogr. D62*, 48–57.

(32) Davis, I. W., Leaver-Fay, A., Chen, V. B., Block, J. N., Kapral, G. J., Wang, X., Murray, L. W., Arendall, W. B., III, Snoeyink, J., Richardson, J. S., and Richardson, D. C. (2007) MolProbity: All-atom contacts and structure validation for proteins and nucleic acids. *Nucleic Acids Res. 35*, W375–W383.

(33) Krissinel, E., and Henrick, K. (2004) Secondary-structure matching (SSM), a new tool for fast protein structure alignment in three dimensions. *Acta Crystallogr. D60*, 2256–2268.

(34) Bulusu, V., Srinivasan, B., Bopanna, M. P., and Balaram, H. (2009) Elucidation of the substrate specificity, kinetic and catalytic mechanism of adenylosuccinate lyase from *Plasmodium falciparum*. *Biochim. Biophys. Acta 1794*, 642–654.